Title
ENHANCED DIFFUSION OF OXYGEN DURING INTERNAL OXIDATION OF NICKEL-BASE ALLOYS

Author
Whittle, D.P.

Publication Date
1981-10-01

LBL-13521
Preprint

Lawrence Berkeley Laboratory
UNIVERSITY OF CALIFORNIA

Materials & Molecular Research Division

Submitted to Philosophical Magazine A

ENHANCED DIFFUSION OF OXYGEN DURING INTERNAL OXIDATION OF NICKEL-BASE ALLOYS

D.P. Whittle, Y. Shida, G.C. Wood, F.H. Stott, and B.D. Bastow

October 1981

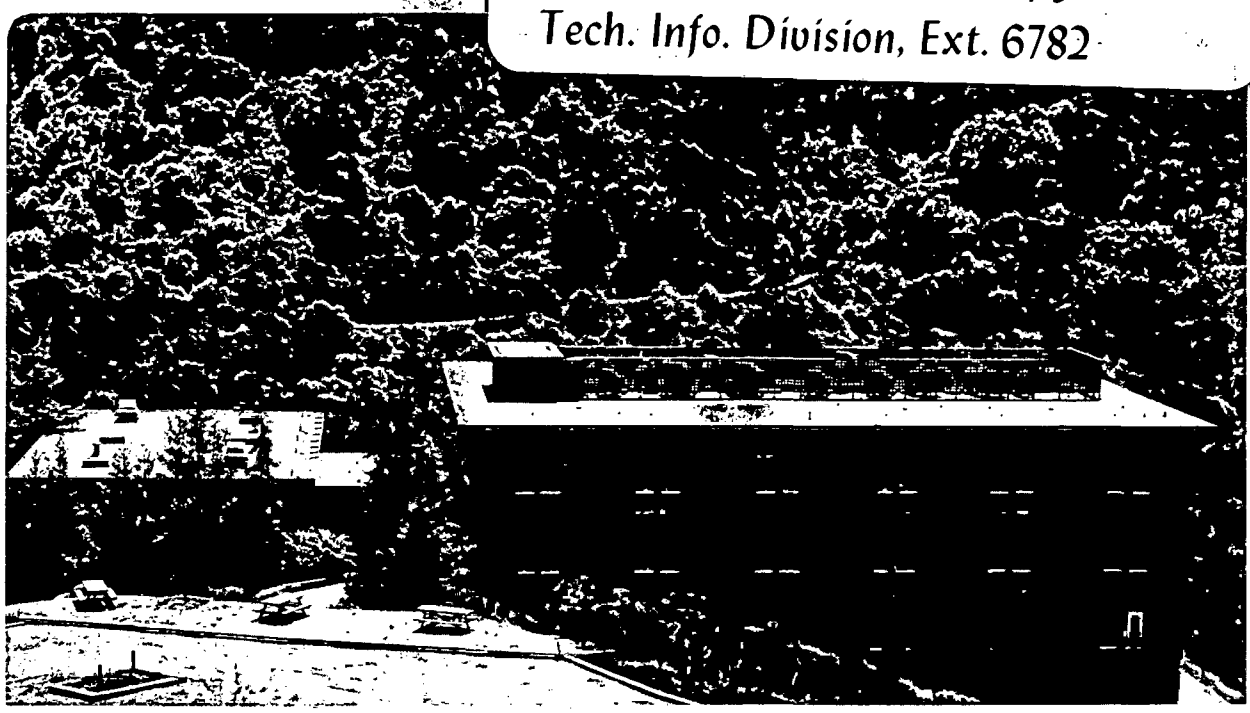

Prepared for the U.S. Department of Energy under Contract W-7405-ENG-48

DISCLAIMER

ENHANCED DIFFUSION OF OXYGEN DURING INTERNAL OXIDATION OF NICKEL-BASE ALLOYS

by

D. P. Whittle
Lawrence Berkeley Laboratory
Department of Materials Science and Mineral Engineering
University of California
Berkeley, California
U.S.A.

Y. Shida
Central Research Laboratories
Sumitomo Metal Industries Ltd.
Amagasaki
Japan

G. C. Wood and F. H. Stott
Corrosion and Protection Center
University of Manchester Institute of Science and Technology
Manchester
England

B. D. Bastow
British Nuclear Fuels
Windscale Works
Seascale, Cumbria
England

The work was carried out at the Corrosion Protection, University of Manchester Institute of Science and Technology, and the authors are greateful to Sumito Metal Industries, Japan for provision of a research grant. The manuscript has been prepared with the support of the Director, Office of Energy Research, Office of Basic Energy Sciences, Material Sciences Division of the U.S. Department of Energy under the Contract No. W-7405-ENG-48. Discussions with Professors R. A. Rapp and W. W. Smeltzer were also useful.

ABSTRACT

The depths of internal oxidation of Ni-Al (0.5-4 wt.%) alloys oxidized in the temperature range 800-1100°C in either Ni/NiO packs or in 1 atm. oxygen is virtually independent of the alloy composition; with Ni-Cr (1.5 wt.%) alloys the depths decrease with increasing Cr content, but to a lesser extent than anticipated by classical theory. A model incorporating enhanced diffusion of oxygen along the incoherent interface between the internal oxide particles and the alloy matrix is proposed. Agreement between experiment and theory is satisfactory if the ratio of diffusion of coefficients in the interface and the bulk lattice is of the order of 10^2-10^3 in the Ni-Al system and approximately 10^4 in the Ni-Cr system. There are also differences between alloys oxidized in Ni/NiO packs, when no surface scale forms and samples oxidized in 1 atm. oxygen when a surface NiO scale also forms. The greater depths of penetration under these latter conditions has been associated with the injection of vacancies into the alloy by the growing surface scale which helps relieve some of the compressive stresses associated with the volume expansion upon internal oxidation, although the exact mechanism is not entirely clear.

Key words: internal oxidation; Ni-Al; Ni-Cr; interfacial diffusion.

§1. INTRODUCTION

The classical model of internal oxidation, as reviewed by Rapp (1965) and others (Meijering 1971, Swisher 1971), has generally been successful in describing the internal oxidation behavior of a wide range of dilute alloys, in which the solute metal forms a more stable oxide than the solvent metal, and in which oxygen has appreciable solubility and diffusivity in the solvent. In essence, oxygen saturates the surface of the alloy, either directly from the atmosphere or by dissociation of the solvent oxide which forms on the surface under the ambient conditions, diffuses inwards and then reacts with the solute element, thus precipitating its oxide. At the advancing internal oxidation front, the supply of reacting atoms is maintained by the inward diffusion of oxygen and the outward migration of solute atoms. Since the solute oxide is very stable, the concentrations of solute remaining dissolved in the alloy within the internal oxidation zone, and of oxygen beyond the internal oxidation zone, should be very low, although measurements by electron probe microanalysis often indicate this is not the case. By solving the transport equations under these conditions, assuming that the previously precipitated internal oxides do not interfere with the inward diffusion of oxygen, the rate of advancement of the internal oxide front can be related to the fundamental variables: oxygen diffusivityin the metallic matrix of the internal oxidation zone, which is essentially pure solvent as outlined above, the metallic interdiffusion coefficient of the alloy, the oxygen solubility of the solvent, the solute content of the alloy, and the stoichiometric ratio of oxygen to solute in the oxide precipitate. Indeed, measurements of internal oxidation rates are frequently used to determine oxygen permeabilities (product of solubility times diffusivity) in metals.

However, in a recent study (Shida 1979) of the behavior of a number of dilute Ni-base alloys, substantial deviations from this classical interpretation of internal oxidation were observed. Two types of internal penetration were observed: a relatively uniform penetration of internal oxidation through the alloy grains, and an enhanced penetration, especially at lower temperatures, along alloy grain boundaries. The oxide precipitates in this latter case are often continuous along the grain boundaries. The present paper describes the kinetics of the uniform type of internal oxidation and

attempts to analyze the discrepancies between the observed rates and those anticipated from the classical theory outlined above, in terms of a model based on enhanced inward penetration of oxygen at the incoherent interfaces between oxide particles and alloy matrix within the internal oxide zone. A subsequent paper (Shida, Whittle, Wood, Stott and Bastow 1981) concentrates on the intergranular oxidation pehnomena and a series of papers (Shida, Stott, Wood, Whittle and Bastow 1981) present more detailed morphological observations.

§ 2. EXPERIMENTAL

The Ni-base alloys used in this investigation were supplied by International Nickel Ltd. and were prepared by rapid vacuum melting. Table I gives the nominal and actual (EPMA) analyses of the alloys prepared from starting materials of the following purities; Ni (99.97%) - 0.008 C, < 0.03 Fe, < 0.002 S, < 0.002 Pb, < 0.001 B, < 0.01 Cr, Co, Mo, Ti, Al, Si, Mn, Zr, Mg, Cu (all in wt.%); Cr - 0.007 N_2, 0.005 C, 0.035 O_2, 0.01 H_2, 0.0003 Pb, 0.0004 Sn, 0.0004 Al, 0.0002 Fe, 0.0004 Na, < 0.0001 Mg, Cu, Ni, Ag, Sb, Bi; Al (99.99%).

All the alloys were hot-rolled to 2 mm strip and then cold-rolled to 0.6 mm strip, from which samples were obtained by cold shearing to a size approximately 20 x 5 mm. Samples were then vacuum annealed in an evacuated and sealed quartz capsule for 5 h at 1200°C; only samples of the same composition were included in each capsule. Optical examination after annealing confirmed virtually inclusion-free alloys, with mean grain sizes as given in Table I. Prior to oxidation, the samples were lightly abraded on 800 and 1200 SiC papers and were electropolished in an orthophosphoric/sulphuric acid solution (420 and 340 ml. respectively in 240 ml. H_2O) at 3.6-4.0 V, 8-12°C and a current density of 0.2-0.4 A/cm^2 for 20 min. They were then etched briefly (5 sec.) in a 5% HF solution.

Internal oxidation was carried out in a "Rhines Pack", using Ni/NiO powder mixtures as the source of oxidant Ni and NiO powders were obtained from Fison's Scientific Apparatus Ltd.; the powders were 99.6% pure, with Fe and Co as the principal impurities. The amount of oxide powder was twice that necessary to oxidize the less noble alloying element in the alloy coupons completely. Only Al-containing alloys, of different Al contents, or Cr-containing alloys, were oxidized simultaneously in the same pack; preliminary experiments indicated that there was no mutual interference between alloy samples of different Al (or Cr) contents. Generally the pack mixture was separate from the samples in the quartz tube.

Some oxidation experiments were also carried out in pure, dry flowing O_2 at 1 atm. pressure, when external scale formation also accompanied the internal oxidation.

Depths of internal oxidation were measured in an optical microscope from metallographically prepared cross-sections, generally in the as-polished

condition. When etching was necessary, a solution of equal parts HNO_3 and glacial acetic acid or 2 parts H_2O/1 part HNO_3/3 parts HCl was used.

§3. EXPERIMENTAL RESULTS

As indicated in §1, two types of internal penetration of oxide were observed in most cases: preferential oxide penetration or precipitation down the alloy grain boundaries, termed intergranular oxidation, and relatively uniform penetration of oxide within the alloy grains. Most of the internal oxide which forms is of the latter sort, and it is the kinetics of this type of internal oxidation with which the present paper is concerned.

Ni-Al Alloys:

Figure 1 shows the depths of the uniform internal oxidation front, measured from the external surface, as a function of time for the various Ni-Al alloys at temperatures in the range 800-1100°C, for samples oxidized in the atmosphere produced by a Ni/NiO Rhines pack. Tentative straight lines have been drawn corresponding to a 1/2 power law dependence of the depth of the internal oxide front, ξ, with time. The real values of this exponent, bearing in mind that these were often calculated from only two data points, fall in the range 0.33 to 0.60, with the lower values generally corresponding to the lower temperatures, although the variation is not especially systematic. A more significant point, however, is that the depth of internal oxidation, after corresponding exposures, decreased slightly with increasing Al content in the alloy at higher temperatures, but was virtually independent of it at lower temperatures.

Experiments carried out in which the samples were in intimate contact with the Rhines pack mixture gave similar depths of internal oxide penetration. However, when the alloys were exposed to 1 atm. oxygen, the depths of internal oxidation were considerably larger than those produced in the Rhines pack, excpet for Ni-0.5 and Ni-1 Al at 800°C. This is shown in Figure 2: except at 1100°C the differences increase with increasing Al content in the alloy. The penetration depths in 1 atm. oxygen have been corrected to allow for the displacement of the original alloy surface inwards due to the simultaneous formation of a NiO surface scale. This is achieved by adding the product of the measured thickness of the external scale and the ratio of the molar volumes of alloy to NiO (=0.61). In addition, however, the internal oxide penetration would be expected to be deeper in the presence of a surface scale since the effective source of the oxidant is moving inwards towards the alloy. As shown later, with all other factors being

equal, the enhancement factor would be given by the ratio $\xi/(\xi-\Delta x)$ where Δx is the displacement of the alloy/scale interface. However, as will be seen later, the observed enhancement is somewhat greater than this.

Ni-Cr Alloys

Similar internal oxide penetration depths versus time plots for the oxidation of dilute Ni-Cr alloys in Ni/NiO packs are shown in Figure 3. Again, tentative lines for a 1/2 power law dependenceare drawn, whilst the actual values fall in a similar range to those for the Ni-Al alloys, namely 0.33-0.6. However, unlike the Ni-Al alloys, the depth of internal oxidation is more strongly dependent on the alloy composition, increasing with decreasing alloy Cr content at all temperatures. A similar dependence was also found when the alloys were oxidized in 1 atm. oxygen, Figure 4, again correcting for the displacement of the original alloy surface. As with the Ni-Al alloys, the depths were all somewhat larger than the corresponding depths formed in the Rhines pack. In the case of the Ni-Cr alloys, however, this can be accounted for by the enhancement factor $\xi/(\xi-\Delta x)$ as will be seen later.

§4. ANALYSIS OF THE DEPTHS OF INTERNAL OXIDATION

According to the classical model (Wagner 1959) of internal oxidation, the rate of penetration of the internal oxide front into the alloy is a parabolic function of time, with

$$\xi = 2\gamma\,(D_0 t)^{\frac{1}{2}} \tag{1}$$

where D_0 is the diffusivity of oxygen in the base metal and γ is a dimensionless parameter dependent on the relative contribution of the diffusion of the component being internally oxidized into the internal oxide zone. γ is obtained by equating the fluxes of oxygen and the internally oxidizing component (designated B) at the precipitation front, which gives the transcendental equation

$$\frac{N_o^{(s)}}{\nu N_B^{(o)}} = \frac{\exp(\gamma^2)\,\operatorname{erf}\gamma}{\phi^{\frac{1}{2}}\exp(\gamma^2\,\phi)\,\operatorname{erfc}\,(\gamma\,\phi^{\frac{1}{2}})} \tag{2}$$

where $N_o^{(s)}$ and $N_B^{(o)}$ are the atomic fractions of dissolved oxygen at the alloy surface and of B in the bulk alloy respectively, and $\phi = D_O/D_B$ the ratio of lattice diffusion coefficients of oxygen to B in the alloy.

Usually, equation (2) is used in one of two limiting forms:
(a) when $\gamma << 1$ and $\gamma\phi^{\frac{1}{2}} >> 1$, equivalent to $D_B/D_O << N_O^{(s)}/N_B^{(o)} << 1$

$$\text{and} \quad \gamma \simeq \left[\frac{N_O^{(s)}}{2\,N_B^{(o)}}\right]^{\frac{1}{2}} \tag{3}$$

and (b) $\gamma << 1$ but $\gamma\phi^{\frac{1}{2}} << 1$, equivalent to $N_o^{(s)}/N_B^{(o)} << D_B/D_O << 1$

$$\text{and} \quad \gamma \simeq \frac{[\pi\phi]^{\frac{1}{2}}\,N_o^{(s)}}{2\nu\,N_B^{(o)}} \tag{4}$$

These two limiting cases also correspond to (a) insignificant diffusion of component B during the internal oxidation process and consequently no enrichment of B in the internally oxidized zone, and (b) significant diffusion of component B and hence its enrichment within the internally oxidized zone respectively.

In order to establish if either limiting case is applicable to the present systems, relevant solubility and diffusivity data from the literature, indicated in Table II, were used. In the Ni-Al system, however, estimations of the ratios D_{Al}/D_O and $N_O^{(s)}/N_B^{(o)}$ were very similar. For

example, at 800°C $D_{Al}/D_O = 2.7 \times 10^{-2}$ and $N_O^{(s)}/N_{Al}^{(o)} = 7.8 \times 10^{-3}$ (for the Ni-4 Al alloy) and 5.7×10^{-2} (for the Ni-0.5 Al alloy). However, as indicated later, D_O may well be altered by the presence of the internal oxide particles, whereas this is unlikely with D_{Al} since aluminum diffusion is only significant, if at all, in the alloy beyond the precipitation front. Thus, a clearer distinction between the two limiting cases is possible using the experimentally determined internal oxide penetration depths. Using equation (1) and the ratio $\phi = D_O/D_{Al}$, it is clearly seen that

$$\gamma = \xi/2\sqrt{D_O t} \quad \text{and} \quad \gamma\phi^{\frac{1}{2}} = \xi/2\sqrt{D_{Al} t}.$$

Re-writing equation (2) as

$$\frac{N_O^{(s)}}{\nu N_B^{(o)}} = \frac{\sqrt{\pi}\,\gamma \exp(\gamma^2)\,\mathrm{erf}(\gamma)}{F(\gamma\phi^{\frac{1}{2}})} \qquad (5)$$

where the function F (n) has been tabulated by Wagner (1959) and noting that under all conditions $\gamma\phi^{\frac{1}{2}} > 2$, and $F(\gamma\phi^{\frac{1}{2}}) > 0.9 \simeq 1$, gives

$$\frac{N_O^{(s)}}{\nu N_B^{(o)}} \simeq \sqrt{\pi}\,\gamma \exp(\gamma^2)\,\mathrm{erf}(\gamma).$$

Using the solubility data in Table II and $\nu = 1.85$ (see later) gives

$$N_O^{(s)}/\nu N_B^{(o)} \simeq \sqrt{\pi}\,\gamma\,\mathrm{erf}\,\gamma \exp(\gamma^2) \leqslant 0.03$$

and hence $\gamma \leqslant 0.14$.

Thus, in the Ni-Al system, the first limiting case is valid: the rate of internal oxidation is governed by the inward diffusion of dissolved oxygen with negligible counterdiffusion of Al.

Concentration profiles of Al and Ni across the internal oxide zones were obtained by electron probe microanalysis. Due to the small size of the internal oxide particles relative to the analyzed region the profiles essentially represent an average Al concentration in the internally oxidized zone. This is little different from the bulk, at least for the dilute alloys, as indicated in the results summarized in Table III. With the more concentrated alloys, especially at 1000 and 1100°C, some enrichment is apparent, although it is unlikely that this has any real significant effect on the subsequent analysis. Interestingly also, the Al concentration at the internal oxide front does not approach zero as implied by the internal oxidation model.

However, this is undoubtedly due to the relatively poor resolution of the electron probe microanalyzer in measuring the very steep concentration profile in that location. A simple calculation for the case of a Ni-4 Al alloy oxidized at 1100°C indicates that the concentration gradient at that location would be approximately 10^3%/μm.

In the Ni-Cr system, the diffusivity of Cr in the alloy is at least one order of magnitude lower than that of Al (see Table II) and, as a consequence, the first limiting case is also valid. Thus, in both cases, the rate of internal oxidation, ξ^2/t, is given by combination of equations (1) and (3) as

$$\frac{\xi^2}{t} = \frac{N_o^{(s)} D_o}{2\nu N_B^{(o)}} \qquad (6)$$

where B represents either Cr or Al. ν, the ratio of oxygen to B component in the stoichiometric precipitate has a value of 1.5 in the Ni-Cr system since the precipitated phase is primarily Cr_2O_3. In the Ni-Al system, however, the spinel phase $NiAl_2O_4$, is formed near to the alloy surface and Al_2O_3 at locations near to the precipitation front. This was confirmed by electron diffraction and electron probe microanalysis of precipitates extracted from sample cross-sections by a replication technique. A sharp transition between spinel and Al_2O_3 was not observed but, for example, for Ni-2.5 Al oxidized at 1000°C, spinel was present up to about 60% through the internal oxide zone.

Meijering (1971) has discussed the formation of internal oxide where the oxide changes to a more stable oxide at a sharp boundary within the internal oxidation zone. In essence, this is equivalent to an effective value of ν given by

$$\nu_{eff} = \frac{\nu_1 (1-F)}{m}$$

where

$$F = \eta/\xi = \frac{[1+4m\ (1-m)(\nu_2-\nu_1)/\nu_1]^{\frac{1}{2}}-1}{2m(\nu_2-\nu_1)/\nu_1}$$

and

$$m = N_0^{(I)}/N_0^{(s)}$$

η is the depth below the surface at which the oxide of stoichiometric ratio ν_1 is formed, ν_2 is the stoichiometry of the oxide precipitate which forms in the region $\eta \leq x \leq \xi$ and $N_0^{(I)}$ is the oxygen concentration at $x = \eta$. m can be calculated from

$$m = N_0^{(I)}/N_0^{(s)} = [P_{O_2}^{(I)}/P_{O_2}^{(s)}]^{\frac{1}{2}}$$

where $P_{O_2}^{(I)}$ and $P_{O_2}^{(s)}$ are the oxygen partial pressures at $x = \eta$ and $x = o$ respectively, corresponding in this case to the Ni-Al_2O_3-$NiAl_2O_4$ and Ni-NiO equilibria respectively. Unfortunately, $P_{O_2}^{(I)}$ is known only at 1000°C, when ν_{eff} is calculated as 1.85 (i.e. the internal oxide is spinel throughout most of the zone). However, a value of ν of 2.0, corresponding to $NiAl_2O_4$ has been used at all temperatures to calculate the permeabilities in the Ni-Al system (Fig. 7). This may give a slight error of less than ∿8%.

Where a surface scale forms simultaneously with the internal oxide, the expression, under the same limiting conditions as equation (6), has been given by Maak (1961) as

$$\frac{\xi(\xi-\Delta x)}{t} = \frac{N_0^{(s)} D_0}{2\nu N_B^{(o)}} \qquad (7)$$

Thus, using the data of the previous section and equations (6) or (7), permeabilities (solubility x diffusivity product) of oxygen in nickel have been calculated. The results are shown in Figures 5 and 6. In the case of the Ni-Al alloys, two important effects emerge:

a) the apparent $N_0^{(s)} D_0$ values increase with increasing Al content in the alloy, and

b) the apparent $N_0^{(s)} D_0$ values obtained from samples oxidized in 1 atm. oxygen (simultaneous NiO formation) are greater under corresponding conditions than those obtained from samples oxidized in Ni/NiO packs.

On the other hand, in the Ni-Cr alloys, the permeability is approximately independent of the alloy composition and, except at 800°C, of the oxidizing conditions. The accuracy of the data at 800°C may be suspect because of the relatively small oxide penetrations involved.

Whatever the reason for the increase in apparent $N_0^{(s)} D_0$ product with increasing alloy Al content, it would be expected that the values should approach a constant value for pure Ni. Tentative extrapolation of the data points for samples oxidized at both 1 atm. and in Ni/NiO packs yields unique values for the permeabilities, and these are re-plotted in Figure 7 and compared with the values for the Ni-Cr system and other values from the literature. Close agreement between these extrapolated data and the data from the Ni-Cr system, and other investigators is apparent.

In order to understand this apparent increase in permeability with increasing Al content in the Ni-Al system, but no similar increase with Cr content in the Ni-Cr system, it is appropriate to consider the morphology of the internal oxide precipitates. These are described in detail elsewhere (Shida et.al. 1981), but in brief, in areas away from the influence of the alloy grain boundaries, where there is relatively uniform penetration through the alloy grains, the immediately noticeable difference is the shape of the precipitates. In the Ni-Al system, the internal oxide particles tend to be acicular in nature, orientated perpendicularly to the original alloy surface, whereas in the Ni-Cr system the particles are more spherical in shape, and also somewhat larger.

It is assumed that the volume fraction of internal oxide precipitate for alloys containing identical amounts of reactive element (Cr or Al) is the same in both systems, and is indeed equal to the atomic fraction of the element present in the original alloy (times the molar volume of oxide to alloy ratio to account for the volume change on oxidation). This was a pre-requisite for using the particular limiting case in analyzing the kinetic data. The size (or number) of the precipitates, and hence the precipitate morphology, is determined principally at the reaction front through the competition for solute atoms between the processes of growth of the existing particles and nucleation of new precipitates. Attempts to analyze this quantitatively (Böhm and Kahlweit 1964) are limited by a lack of knowledge of the degree of supersaturation required for precipitation to occur. Nevertheless, depending on the size and shape of the individual particles, the ratio of interfacial area (between oxide particle and matrix) to volume will vary. For example, a typical, spherical Cr_2O_3 particle of 1 μm radius and a plate-like Al_2O_3 particle of 0.1 μm thick, 0.3 μm wide and 140 μm long (identical volume) would have surface areas of 1.3×10^{-7} and 1.1×10^{-6} cm^2 respectively. This difference would be even further exaggerated if the volume of the individual Al_2O_3 precipitates were smaller, with a consequent increase in their total number to give the same total volume fraction. If then enhanced diffusion along the incoherent boundary between oxide particle and alloy matrix is significant, it would be much more significant in the Ni-Al alloys than in the Ni-Cr alloys. A model incorporating this premise is advanced in the next section.

§5. INTERNAL OXIDATION MODEL INVOLVING ENHANCED OXYGEN DIFFUSION

The basic thesis of the model is that oxygen diffusion within the internal oxidation zone is enhanced along the incoherent interface between the internal oxide particles and the alloy matrix. As a consequence, the effective flux of oxygen through the internal oxide zone is considered as the sum of the fluxes of oxygen through the alloy lattice, J_l, the internal oxide/alloy interface, J_i, and the internal oxide particles themselves, J_{ox} as shown in the schematic diagram, Figure 8. Thus,

$$J_{eff} = J_l A_l + J_i A_i + J_{ox} A_{ox} \qquad (8)$$

where A_l, A_i and A_{ox} are the area fractions of alloy phase, interface and oxide in a unit cross-section cut parallel to the external surface. The third term may be neglected since oxygen diffusivities in the oxide phase are very small in comparison to those in the alloy lattice and the interface. Indeed, the oxide phase may have a blocking effect on the inward diffusion of oxygen, although if A_{ox} is small, this can be considered negligible.

If it is assumed that the distance over which lateral diffusion (parallel to the external surface is relatively small in comparison with distances normal to the external surface),the oxygen concentration gradient in the interface can be regarded as identical to that in the alloy and a uniform concentration at any distance x from the external surface can be considered. Then the effective diffusion coefficient for oxygen in the internal oxidation zone is defined as

$$D_{O,eff} = D_{O,l} A_l + D_{O,i} A_i \qquad (9)$$

where $D_{O,l}$ is the lattice diffusion coefficient of oxygen and $D_{O,i}$ the interfacial diffusion coefficient. Both these coefficients are assumed independent of composition.

The area fractions, A_l and A_i, depend, among other factors, on the morphology of the internal oxide precipitates. Initially, consider the limiting case where the internal oxides take the form of platelets orientated in the growth direction, which approximates to the morphology observed in the Ni-Al system. The thickness and width of the platelets are designated d and w respectively, (see Figure 8) and it is assumed they extend continuously through the internal oxide zone, which extends to a depth ξ below the surface, although this latter assumption does not affect the final result since in effect the average flux through a unit plane parallel to the surface

is being considered; local lateral variations in the oxygen flux are not considered. If N_{BO_ν} is taken as the mole fraction of oxide, BO_ν, relative to the total number of moles of alloy constituents within the internal oxide zone then, by considering a volume of internal oxide zone of thickness ξ and unit cross-sectional area, the number of platelets of oxide, Z may be calculated:

$$\frac{N_{BO_\nu} \cdot \xi}{V_{all}} = Z \frac{w.d.\xi}{V_{ox}} \qquad (10)$$

where V_{ox} and V_{all} are the molar volumes of oxide and alloy phases respectively. The volume expansion due to internal oxide precipitation has been neglected. Thus,

$$Z = \frac{V_{ox}}{V_{all}} \frac{N_{BO_\nu}}{w.d} \qquad (11)$$

and the fractional area of interface is given as

$$A_i = 2(w+d).Z.\delta_i \approx 2wZ\delta_i \qquad (12)$$

where δ_i is considered as the width of the interface. The approximation may be used if the platelets are thin, $d \ll w$.

Clearly, the fractional cross-sectional area of lattice available for diffusion is given by

$$A_l = 1-A_i-A_{ox} = 1 - 2wZ\delta_i - Zwd \qquad (13)$$

Thus, substituting equations (11)-(13) in equation (9) gives

$$D_{O,eff} = D_{O,l} \left[1 - \frac{V_{ox}}{V_{all}} N_{BO_\nu} \left(1+2 \frac{\delta_i}{d}\right)\right] + 2D_{O,i} \frac{V_{ox}}{V_{all}} N_{BO_\nu} \frac{\delta_i}{d} \qquad (14)$$

which on re-arrangement gives

$$\frac{D_{O,eff}}{D_{O,l}} = 1 + \left[2 \frac{\delta_i}{d} \left(\frac{D_{O,i}}{D_{O,l}} - 1\right) - 1\right] \frac{V_{ox}}{V_{all}} N_{BO_\nu} \qquad (15)$$

This can be further approximated since $D_{O,i} \gg D_{O,l}$:

$$\frac{D_{O,eff}}{D_{O,l}} = 1 + \left[\frac{D_{O,i}\delta_i}{D_{O,l}} \cdot \frac{2}{d} - 1\right] \frac{V_{ox}}{V_{all}} N_{BO_\nu} \qquad (16)$$

Thus, the effective diffusion coefficient in the internal oxide zone is a linear function of the mole fraction of internal oxide precipitate, which in

the present limiting case is identical to the original atom fraction of B in the original alloy.

Equation (16) holds for the limiting case defined earlier, namely for the formation of acicular platelets of internal oxide. However, a similar expression is obtained for other internal oxide morphologies. For example, if the internal oxides consist of randomly distributed spherical particles of radius r, then

$$\frac{D_{O,eff}}{D_{O,l}} = 1 + \left[\frac{D_{O,i}\delta_i}{D_{O,l}} \cdot \frac{3}{r} - 1\right] \frac{V_{ox}}{V_{all}} N_{BO_\nu} \qquad (17)$$

which is identical to equation (10) except for 3/r replacing 2/d.

The left hand side of equation (16), or equation (17), can be written as

$$\frac{N_O^{(s)} D_{O,eff}}{N_O^{(s)} D_O} = 1 + \left[\frac{D_{O,i}\delta_i}{D_{O,l}} \cdot \frac{2}{d} - 1\right] \frac{V_{ox}}{V_{all}} N_{BO_\nu} \qquad (18)$$

If it is assumed that the solubility of oxygen at the surface is not affected by the presence of Al in the alloy, and this is usually accepted since the alloy matrix is in all cases virtually pure Ni, then the ratio on the left side of equation (18) corresponds to the ratio of the apparent $N_O^{(s)} D_O$ product (Figure 5) to the value obtained by extrapolating to pure Ni. This is plotted in Figure 9 for the data obtained from oxidation in Ni/NiO packs and at 1 atm. of oxygen.

The ratios are an approximate linear function of the solute mole fraction in accord with equation (8), at least for samples oxidized by the Ni/NiO packs. However, in the case of oxidation in 1 atm. oxygen, the ratios increase rapidly with increasing Al content.

In order to test the model further, it is necessary to examine whether the parameters in equation (16) are physically reasonable. The gradients of the best fit lines through the data points are given in Table IV. These correspond to

$$\left(\frac{D_{O,i}\delta_i}{D_{O,l}} \cdot \frac{2}{d} - 1\right) \frac{V_{ox}}{V_{all}}$$

Assuming all the internal oxide particles were spinel, $NiAl_2O_4$, then V_{ox} = 19.5 cm^3 and V_{all} = 6.67 cm^3, and $\frac{D_{O,i}\delta_i}{D_{O,l}}$ can be calculated and is given in Table IV. Usually, the width of grain boundaries in studies of grain boundary diffusion is taken as several interatomic distances, thus δ_i is approximated to 10 Å. The thickness of the internal oxide particles, d, varies with

temperature and alloy content but lies in the range 100-1000 Å. Thus, $D_{O,i}/D_{O,l}$ ratios have values in the range 4×10^2-10^4 as indicated in Table IV, with the ratio increasing with decreasing temperature as might be expected. Unfortunately, no measurements for oxygen diffusion along grain boundaries have been made for comparison. Self diffusion coefficients for Ni diffusion via lattice (Adda and Philibert 1966) and grain boundaries (Martin and Peraillon 1975) are available, and the ratio $D_{Ni,i}/D_{Ni,l}$ has values of 2.3×10^4 and 1.1×10^6 at 1100 and 800°C respectively. However, it must be remembered that oxygen is presumed to diffuse via an interstitial mechanism as opposed to a substitutional mechanism as in the case of Ni and consequently, the presence of disordered, incoherent interfaces would be expected to produce a somewhat smaller enhancement in the diffusion coefficient.

Turning to the Ni-Cr alloys, the ratio of apparent $N_O^{(s)}D_O$ to $(N_O^{(s)}D_O)_{pure\ Ni}$ is plotted as a function of atomic fraction of Cr content in Figure 10. The data do not fit a linear relationship as well as those for the Ni-Al alloys. Nevertheless, tentative gradients were measured (Table IV) and using appropriate values for V_{ox} (14.5 cm^3), δ_i(10 Å) and equation (17) with r, the radius of the spherical particles of 1, 0.5, 0.3 and 0.2 μm at 1100, 1000, 900 and 800°C respectively gives a $D_{O,i}/D_{O,l}$ ratio of around 1-2 $\times 10^4$, and virtually independent of temperature (Table IV).

§6. DISCUSSION

Permeability values for oxygen in Ni determined by internal oxidation measurements on dilute alloys are invariably higher than values obtained from independently measured oxygen solubility and diffusivity, (Figure 7,8) and this has been attributed, in the present systems, to the enhanced diffusivity of oxygen down the incoherent interface between the matrix and the internal oxide particles. However, other explanations have been put forward. According to Rapp (1964, 1965), Al-O cluster formation or precipitation of non-stoichiometric oxides can alter the $N_O^{(s)} D_O$ product. The effect is considered to be particularly important when internal oxidation causes precipitation of very small oxide particles, as with dilute alloys. However, small changes in the stoichiometric ratio, ν, are considered unlikely to cause the relatively large changes in the apparent permeabilities measured in the present work.

An additional factor may be the possibility of ternary interactions (Smeltzer and Whittle 1978). The alloy containing dissolved oxygen is in effect a ternary system and as a consequence two additional factors should be considered. Firstly, the oxygen solubility may vary with alloy content, although it is usually assumed that when a very stable oxide such as Al_2O_3, is precipitated, then the residual Al content in the alloy, especially at the surface, is negligible. Unfortunately, independent oxygen solubility measurements, and their dependence on alloy composition, or purity, are difficult to achieve.

The second factor is related to the driving force for diffusion really being the activity gradient, rather than the concentration gradient. This means that the oxygen flux is dependent both on its own concentration gradient and that of the solute element, especially where there is strong thermodynamic interaction. Smeltzer and Whittle (1978) showed that under conditions where the concentration of solute element remaining in the internal oxide zone was considerable (i.e. when the surface scale and internal oxide precipitate were the same phase) the driving force provided by the solute concentration profile for exceeded that due to oxygen concentration gradient itself. Nevertheless, under the conditions of the present experiments where the residual Al content in the alloy after oxide precipitation is negligible, then the ternary interaction effect can also be neglected.

According to the present model, differences in apparent $N_0^{(s)}D_0$ products between the various alloy systems has been related to differences in internal oxide morphology, and it is perhaps appropriate to discuss briefly the factors which affect this morphology. According to Böhm and Kahlweit (1964), at the internal oxidation front there is a competition between the growth of the existing precipitates and the nucleation of new particles, both processes resulting in advance of the oxidation front. The nucleation of new particles depends on the degree of supersaturation in advance of the existing particles and is determined by the relative magnitudes of the oxygen and solute fluxes at that point. High oxygen fluxes, such as when the zone of internal oxide is thin, result in repeated nucleation and the individual particle size is relatively small. On the other hand, when the oxygen flux diminishes as the internal oxide zone grows thicker, the existing particles tend to grow in size, often elongated in the growth direction. Thus, even for a given system under fixed exposure conditions, there is considerable size range to the individual oxide particles, varying from small and spherical near to the alloy surface to large and elongated at greater depths into the alloy. A cubic relationship with distance below the surface is suggested (Böhm and Kahlweit, 1964).

This dependence of precipitate size with distance into the alloy has not been included in the present analysis. However, there are other factors which affect the precipitate size to perhaps a greater extent, namely the flux of the solute element to the precipitation front. Generally, the greater the solute content, the greater is the flux and hence the greater the tendency to form larger particles. The diffusion coefficient in the alloy is also important. In the Ni-Al system, this is at least an order of magnitude greater than in the Ni-Cr system, and as a consequence, the oxide particles adopt an acicular shape, which maximizes the interfacial area between particle and matrix. Indeed, Hindam and Smeltzer (1980) suggest that the Al_2O_3 formed internally in dilute Ni-Al alloys consists entirely of continuous rods oriented normally to the alloy surface.

Surprisingly, however, there are no marked differences in internal oxide morphology between samples oxidized in Ni/NiO packs and at 1 atm. O_2 pressure. Nevertheless, there is a considerable increase in the apparent $N_0^{(s)}D_0$ product for Ni-Al alloys under the latter conditions. At least two explanations are possible, although neither can be substantiated quantitatively. Firstly, there appears to be differences in the population densities of precipitated

oxide particles under the two conditions, and whilst this is not expected under the assumptions of the analysis given earlier, the observations in the electron microscope (Shida et.al. 1981) indicate a greater population density of precipitates in samples oxidized in the Rhines pack compared with corresponding alloys oxidized in 1 atm. oxygen. This could give rise to a blocking effect, compensated by a reduction in the inward flux of dissolved oxygen from the Rhines pack, and hence the apparent $N_O^{(s)}D_O$ product. It might also be appropriate to guery whether the Rhines pack can supply oxygen sufficiently rapidly to maintain oxygen saturation at the alloy surface, although this does not appear to have been questioned by other workers.

The second possibility is that of vacancy injection into the alloy as a result of forming NiO on the surface (Hancock and Fletcher 1966, Douglass 1968) which plays some role, although the detailed mechanism is not clear. Enhancement of the oxygen diffusivity in the alloy by the injection of vacancies, however, would not normally be expected since oxygen diffuses by an interstitial mechanism. If, on the other hand, the injected vacancies condense at the internal oxide/metal interface, then they may decrease the degree of coherency at that interface, increasing its effective width. Although, it should be noted that the discrepancy between apparent $N_O^{(s)}D_O$ products from samples oxidized in Ni/NiO packs and 1 atm. O_2 is largest at the lower temperatures, where surface oxidation, and hence vacancy injection, is smaller.

Vacancy injection into the alloy as a result of surface oxidation may also help relieve the compressive stresses induced within the internal oxidation zone by the volume expansion associated with precipitation. However, whether the metallic lattice could retain stress at all at these elevated temperatures is open to question. Indeed, extrusion of the nickel matrix at the surface of the sample has been noted (Shida et.al. 1981).

Finally, it is appropriate to mention the possibility that at the internal oxidation front not all the incoming oxygen flux is consumed in precipitating oxide. On a microscopic scale, this may well be true. Once an oxide particle is precipitated the matrix immediately surrounding the particle is depleted in the solute and as a consequence only a fraction of the oxygen flux through that region is required for growth of the precipitate since this is limited by the diffusion of the solute element. In effect, this means that the width of the interfacial region around the precipitate

through which the oxygen flux can pass unimpeded is of the order of microns (width of the diffusion-limited solute-depletion zone) rather than the 10 Å or so associated with the structural incoherency of the interface. However, these arguments are only valid on a localized, microscopic scale. The macroscopic rate of advancement of the internal oxide precipitation front would be unaffected, unless substantial amounts of unreacted solute remained within the zone of internal oxidation. This is difficult to establish directly by experiment, but would also imply that the volume fraction of internal oxide was substantially less than the original atom fraction of solute in the alloy. This is definitely not observed experimentally. However, the idea of an unimpeded oxygen flux due to solute depletion may well be more relevant in discussing enhanced intergranular penetration as will be shown in a later paper (Shida et.al. 1981).

§7. ACKNOWLEDGEMENTS

The work was carried out at the Corrosion Protection Center, University of Manchester Institute of Science and Technology, and the authors are grateful to Sumito Metal Industries, Japan for provision of a research grant. The manuscript has been prepared with the support of the Director, Office of Energy Research, Office of Basic Energy Sciences, Material Sciences Division of the U.S. Department of Energy under the Contract No. W-7405-ENG-48. Discussions with Professors R. A. Rapp and W. W. Smeltzer were also useful.

§8. REFERENCES

ADDA, Y., and PHILIBERT, J., 1966 "La Diffusion dans les Solides," (Press Universite de France).

BÖHM, G., and KAHLWEIT, M., 1964, Acta Met., 12, 641.

DOUGLASS, D.L., 1968, Corros. Sci., 8, 665.

GOTO, S. and KODA, S., 1968, J. Japan Inst. Met., 32, 334.

HANCOCK, A., and FLETCHER, R., 1966, Metallurgia, 6, 1.

HINDAM, H., and SMELTZER, W. W., 1980, J. Electrochem. Soc., 127, 1622.

MAAK, F., 1961, Z. Metallkunde, 52, 545.

MARTIN, G., and PERRAILLON, B., 1975, J. Phys. Colloq., 4, 165.

MEIJERING, J. L., 1971, "Adv. in Materials Research," 5, 1 (ed. H. Herman, Academic Press).

RAPP, R. A., 1965, Corrosion, 21, 382.

SEYBOLT, A. U., 1976, quoted in "Metals Ref. Book" (ed. C. J. Smithells, 5th ed., Butterworths).

SHIDA, Y., 1979, Ph.D. Thesis, University of Manchester.

SHIDA, Y., STOTT, F. H., WOOD, G. C., WHITTLE, D. P., and BASTOW, B. D., 1981, to be published.

SHIDA, Y., WHITTLE, D. P., WOOD, G. C., STOTT, F. H., and BASTOW, B. D., 1981, to be published.

SCHWARZKOPF, W. M., 1959, Z. Elektrochem., 63, 830.

SMELTZER, W. W., and WHITTLE, D. P., 1978, J. Electrochem. Soc., 125, 1116.

SMITHELLS, C. J., and RANSLEY, C. E., 1936, Proc. Roy. Soc., A155, 195.

STOTT, F. H., and WOOD, G. C., 1977, Corros. Sci., 17, 647.

SWALIN, R. A. and MARTIN, A., 1956, Trans. AIME, 206, 567.

SWISHER, J. H., 1971, "Oxidation of Metals and Alloys" (ed. D. L. Douglass, ASM), 235.

VERFURTH, J. E., and RAPP, R. A., 1964, Trans. AIME, 230, 1310

WAGNER, C., 1959, Z. Elektrochem., 63, 772.

TABLE I. Compositions of Nickel-Base Alloys

Nominal Compn.(w/o)	Actual(EPMA) Compn.(w/o) Al	Cr	Grain Size (μm)
Ni-0.5 Al	0.55	<0.01	610
Ni-1 Al	1.15	0.02 - 0.05	320
Ni-2.5 Al	2.45	<0.01	480
Ni-4 Al	4.10	<0.01	620
Ni-1 Cr	--	1.10	690
Ni-2 Cr	<0.01	2.00	640
Ni-3 Cr	<0.01	3.00	360
Ni-5 Cr	<0.01	4.66	440

TABLE II. Solubility and Diffusivity Values in Ni-Base Alloys

Temp.°C	Solubility of O_2 in Ni (Seybolt 1976)	Diffusivity of O_2 in Ni, cm^2/s (Smithells and Ransley 1936)	Diffusivity of Al in Ni, cm^2/s (Swalin and Martin 1936)	Diffusivity of Cr in Ni(10),cm^2/s (Adda and Philibert 1966)
1100	4.8×10^{-4}	2.5×10^{-8}	1.2×10^{-10}	4.7×10^{-11}
1000	5.1×10^{-4}	2.4×10^{-9}	1.9×10^{-11}	7.2×10^{-12}
900	6.0×10^{-4}	1.5×10^{-10}	2.2×10^{-12}	8.0×10^{-13}
800	6.9×10^{-4}	6.3×10^{-12}	1.7×10^{-13}	5.9×10^{-14}

TABLE III. Average Al Concentrations in the Internal Oxide Zone and at the Advancing Internal Oxidation Front

Oxidizing Condns.	Alloy	Av. Al in IO Zone(%)	Enrichment Factor	Al Conc. at IO Front(%)
	Ni-0.5Al	0.57	1.03	0.4
10h at 1100°C	Ni-1 Al	1.2	1.04	0.7
	Ni-2.5Al	3.3	1.3	0.9
	Ni-4 Al	5.5	1.3	1.0
20h at 1000°C	Ni-1 Al	1.3	1.1	0.5
	Ni-2.5Al	3.8	1.6	1.1
40h at 900°C	Ni-1 Al	1.15	1	0.6
160h at 800°C	Ni-0.5Al	0.55	1	0.4
	Ni-1 Al	1.15	1	0.8
	Ni-2.5Al	2.9	1.2	1.5

TABLE IV. Calculation of the Parameter $\left(\frac{D_{O,i}\delta_i}{D_{O,1}}\right)$ for Ni-Al and Ni-Cr Alloys

Temp.,°C	Ni-Al $\frac{D_{O,i}\delta_i}{D_{O,1}}$	Ni-Al $\frac{D_{O,i}}{D_{O,1}}$	Ni-Cr $\frac{D_{O,i}\delta_i}{D_{O,1}}$	Ni-Cr $\frac{D_{O,i}}{D_{O,1}}$
1100	39	$4.9 - 10.0 \times 10^2$	16-19	$1.6 - 1.9 \times 10^4$
1000	85	$8.5 - 10.0 \times 10^2$	25-34	$1.2 - 1.7 \times 10^4$
900	85	$8.5 - 10.0 \times 10^2$	34-59	$1.0 - 1.8 \times 10^4$
800	173	$1.7 - 10.0 \times 10^3$	77-246	$1.5 - 4.9 \times 10^4$

FIGURE CAPTIONS

Figure 1. Uniform internal oxidation depth-time realtionships for Ni-Al alloys oxidized in Ni-NiO Rhines packs.

Figure 2. Comparison of the depths of internal oxidation zones in Ni-Al alloys oxidized at 1 atm. O_2 and in Ni/NiO packs.
a) 10h at 1100°C; b) 20h at 1000°C; c) 40h at 900°C;
d) 160h at 800°C.

Figure 3. Uniform internal oxidation depth-time relationships for Ni-Cr alloys oxidized in Ni/NiO Rhines packs.

Figure 4. Comparison of the depths of internal oxidation zones in Ni-Cr alloys oxidized at 1 atm. O_2 and in Ni/NiO packs.
a) 10h at 1100°C; b) 20h at 1000°C; c) 40h at 900°C;
d) 160h at 800°C.

Figure 5. Apparent $N_O^{(s)} D_O$ products calculated from the depths of internal oxidation in Ni-Al alloys oxidized in 1 atm. O_2 and Ni/NiO packs.

Figure 6. Apparent $N_O^{(s)} D_O$ products calculated from the depths of internal oxidation in Ni-Cr alloys oxidized in 1 atm. O_2 and Ni/NiO packs.

Figure 7. Comparison of permeability data for oxygen in Ni with other values.

Figure 8. Schematic diagram of the internal oxidation model.

Figure 9. Ratio of apparent permeability of permeability in pure Ni for Ni-Al alloys oxidized in Ni/NiO packs and 1 atm. O_2.

Figure 10. Ratio of apparent permeability to permeability in pure Ni for Ni-Cr alloys oxidized in Ni/NiO packs and 1 atm. O_2.

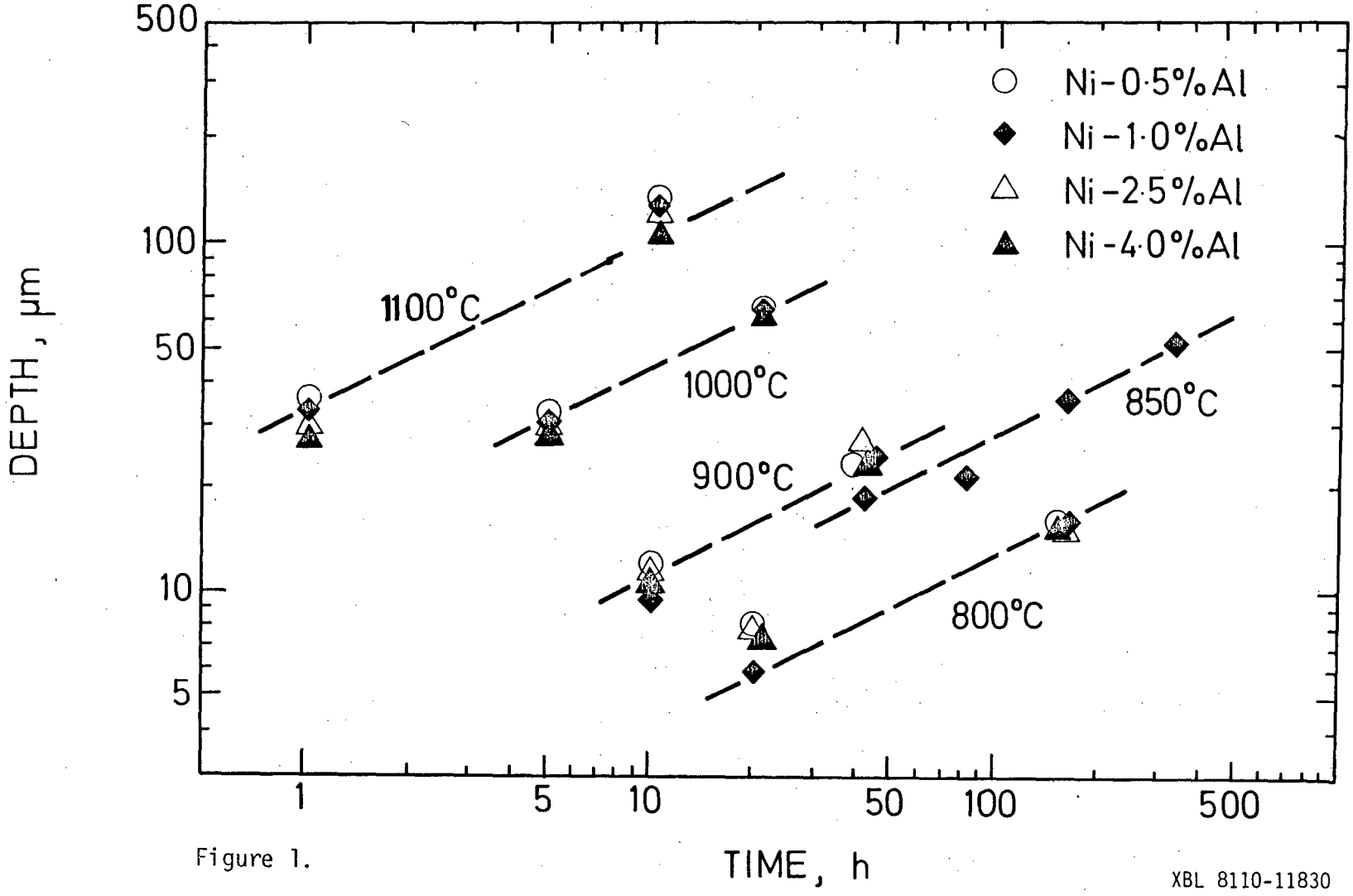
500
100
50
10
5
DEPTH, μm
1
5
10
50
100
500
TIME, h
Ni-0·5%Al
Ni-1·0%Al
Ni-2·5%Al
Ni-4·0%Al
1100°C
1000°C
900°C
850°C
800°C
XBL 8110-11830

Figure 1.

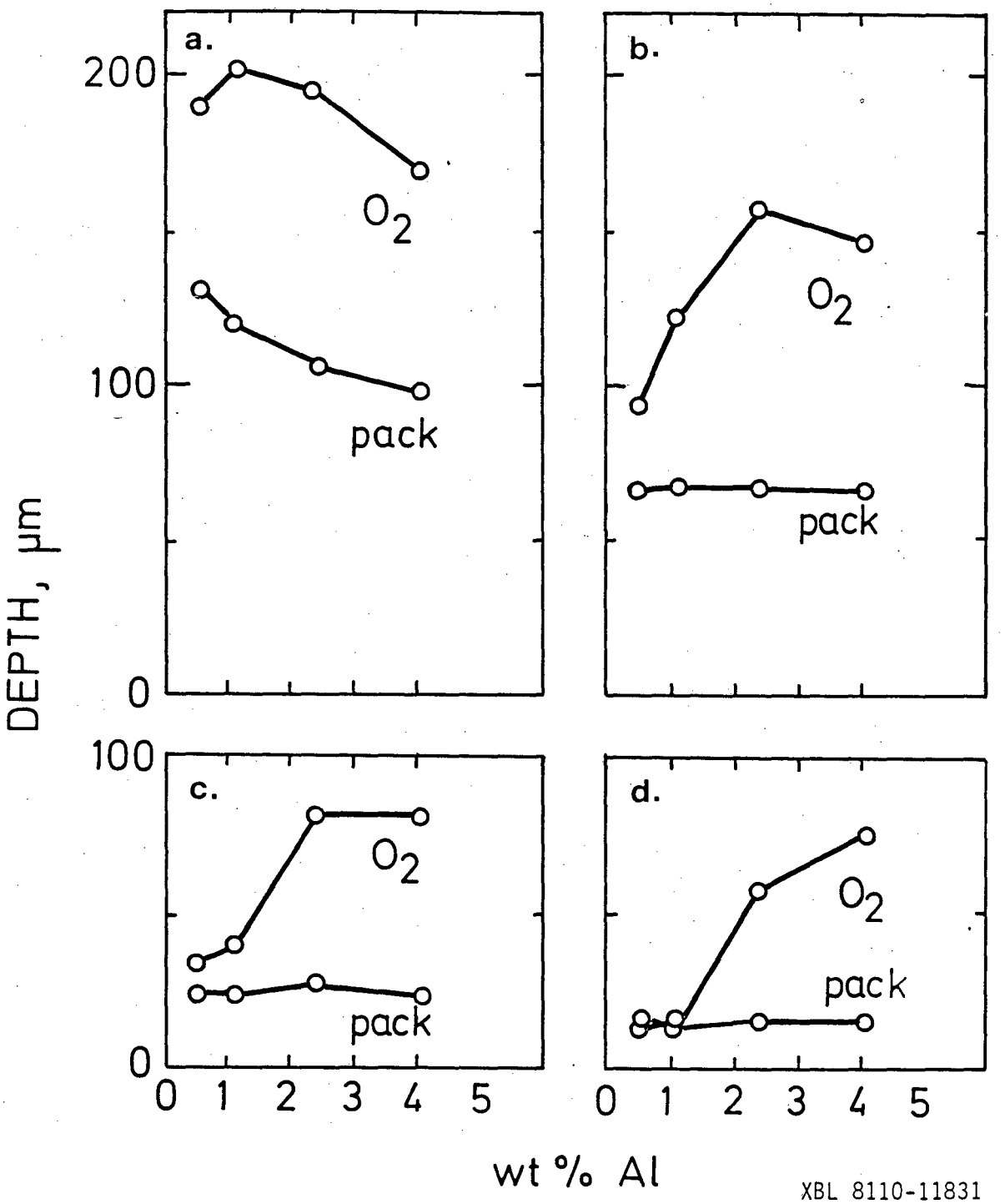
a.
b.
c.
d.
200
100
0
100
0
O_2
pack
DEPTH, μm
0 1 2 3 4 5
wt % Al
XBL 8110-11831

Figure 2.

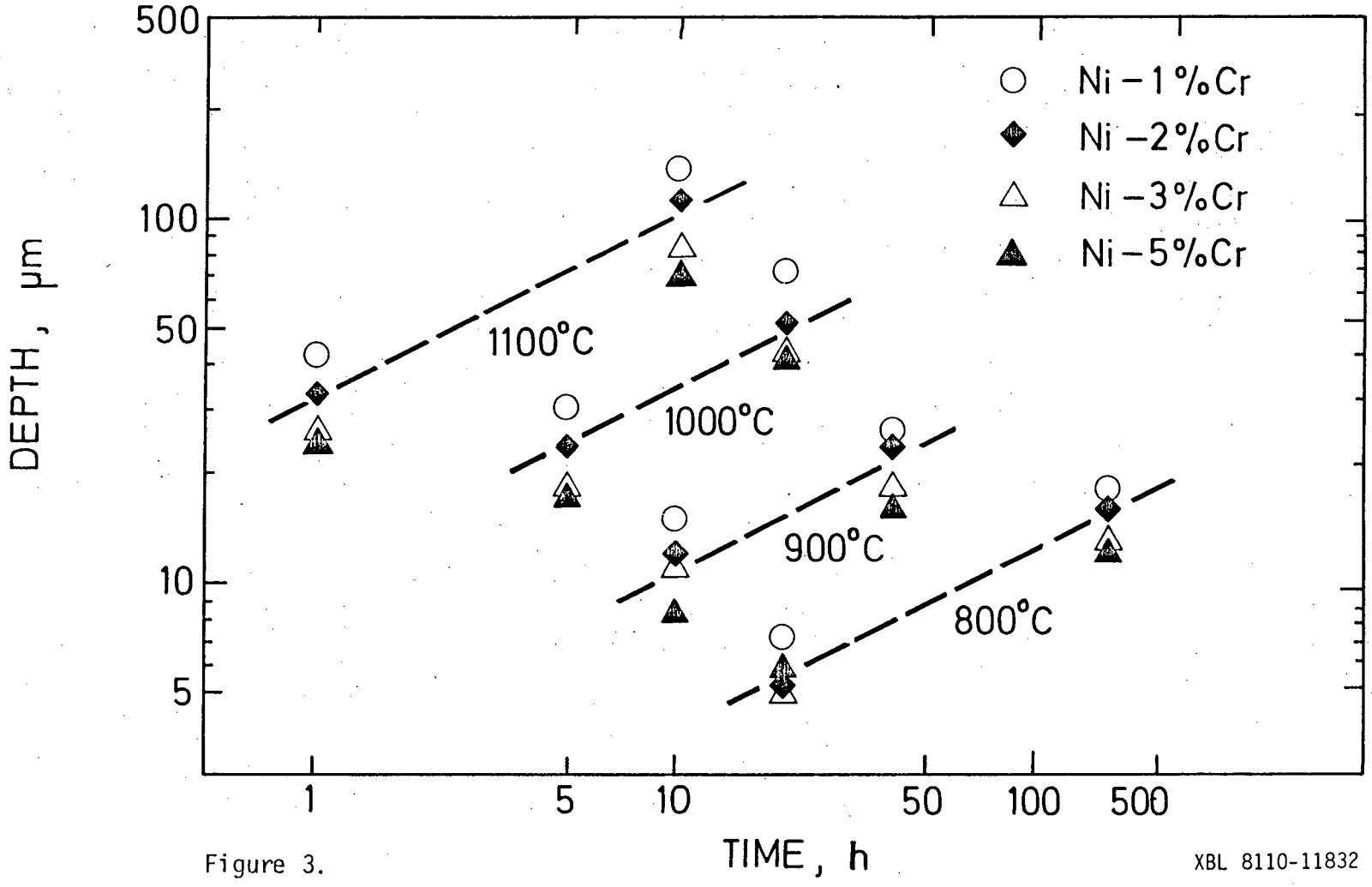

Figure 3.

XBL 8110-11832

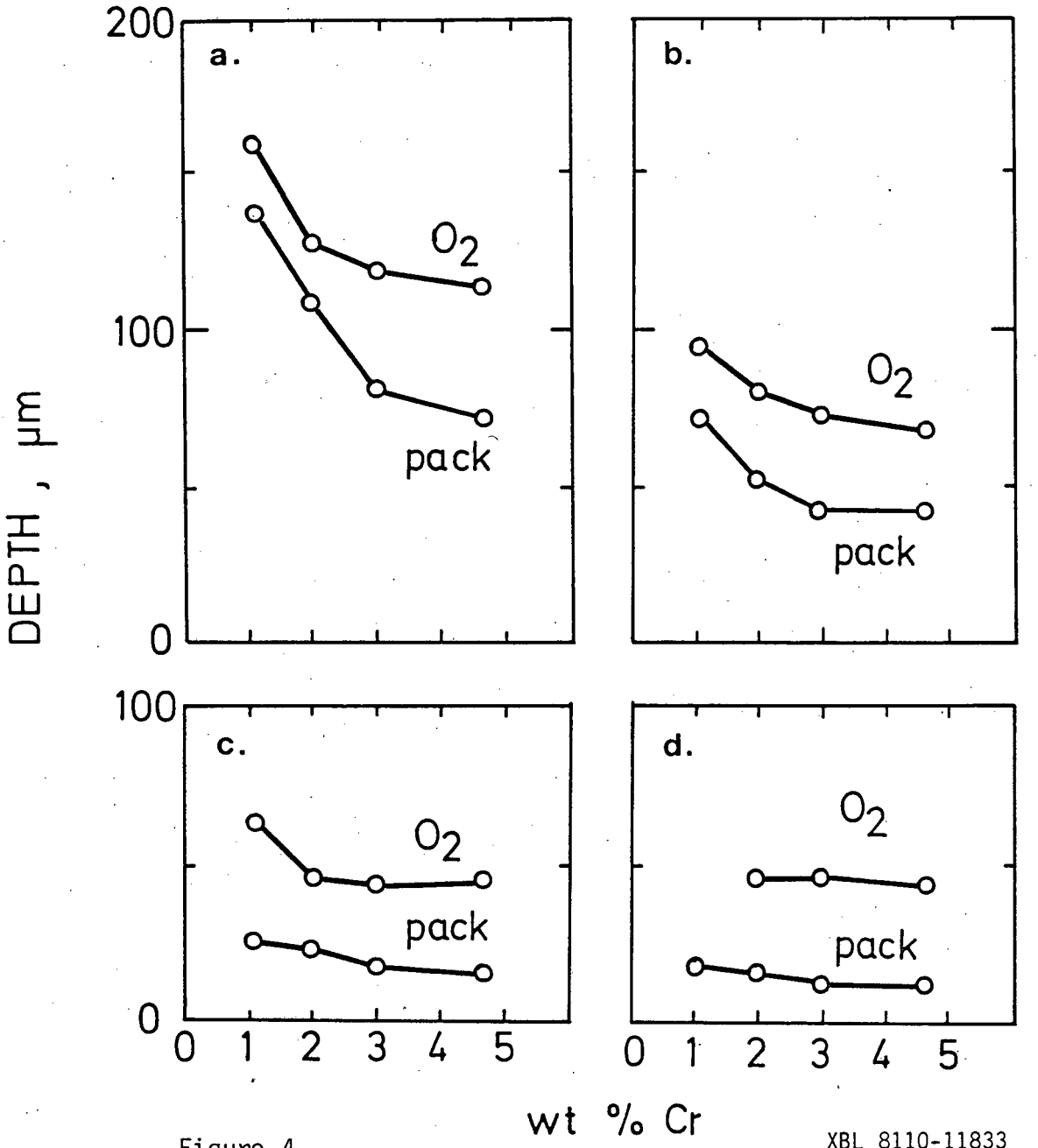

Figure 4.

XBL 8110-11833

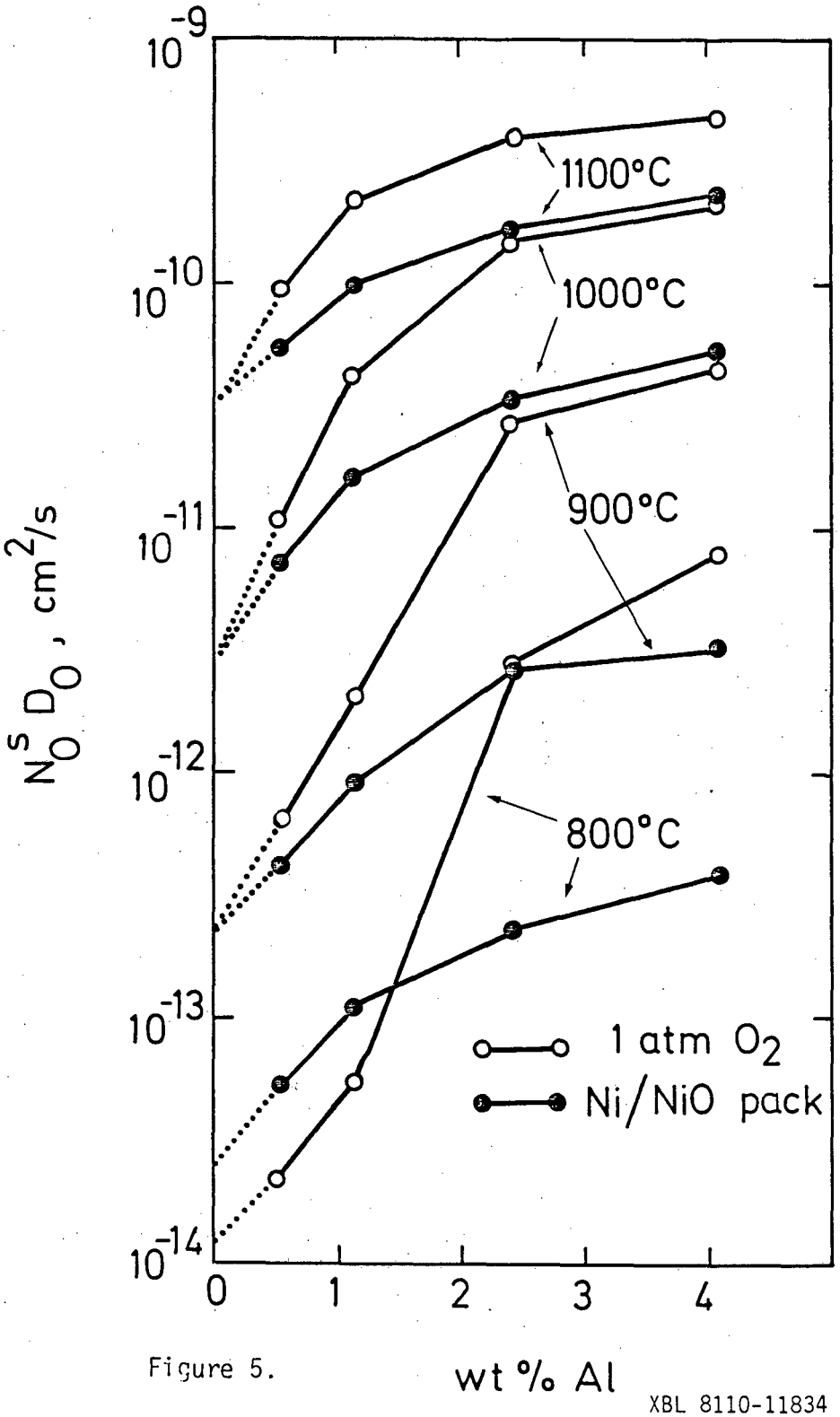

Figure 5.

XBL 8110-11834

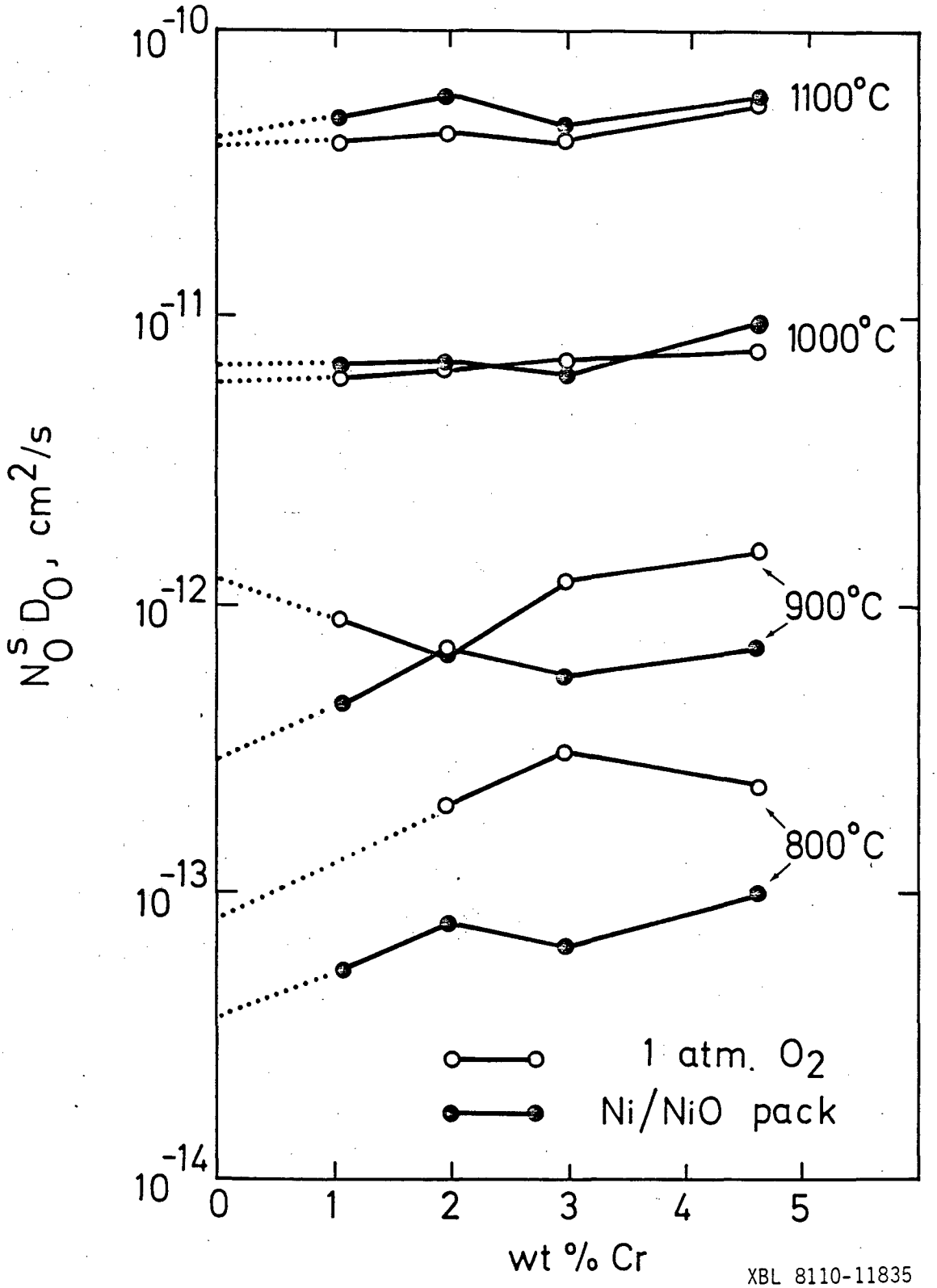
10^{-10}
10^{-11}
10^{-12}
10^{-13}
10^{-14}
$N_O^s D_O$, cm^2/s
1100°C
1000°C
900°C
800°C
1 atm. O_2
Ni/NiO pack
0
1
2
3
4
5
wt % Cr
XBL 8110-11835

Figure 6.

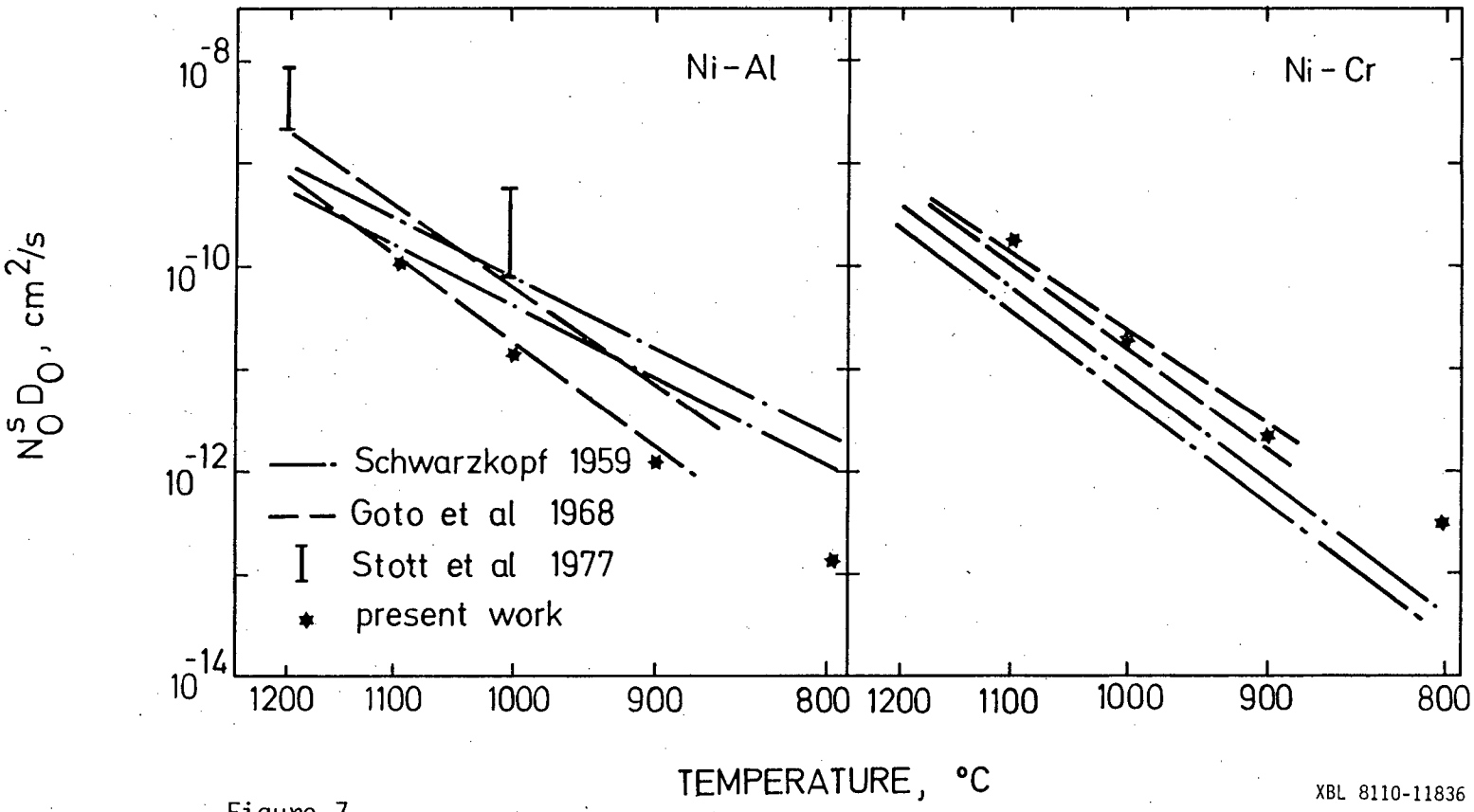
Ni-Al
Ni-Cr
10^{-8}
10^{-10}
10^{-12}
10^{-14}
$N_O^S D_O$, cm^2/s
Schwarzkopf 1959
Goto et al 1968
Stott et al 1977
present work
1200
1100
1000
900
800
TEMPERATURE, °C
XBL 8110-11836

Figure 7.

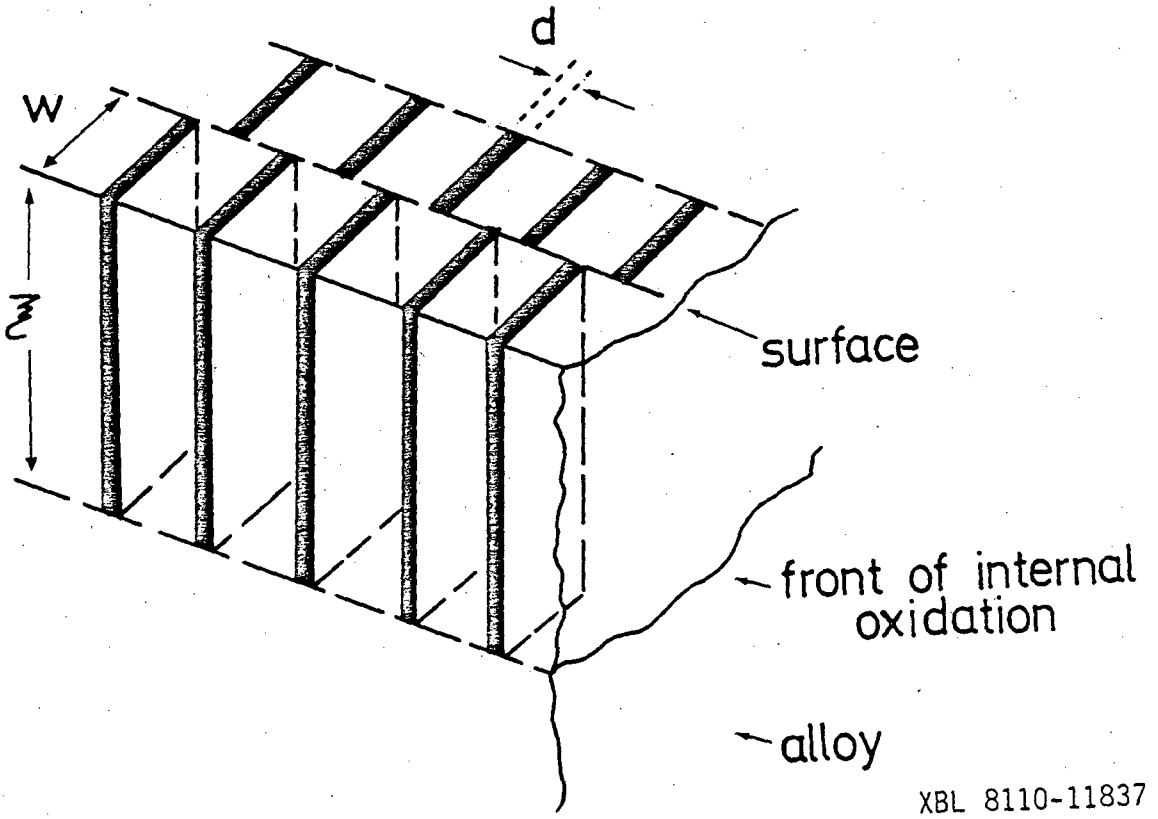
d
W
surface
front of internal oxidation
alloy
XBL 8110-11837

Figure 8.

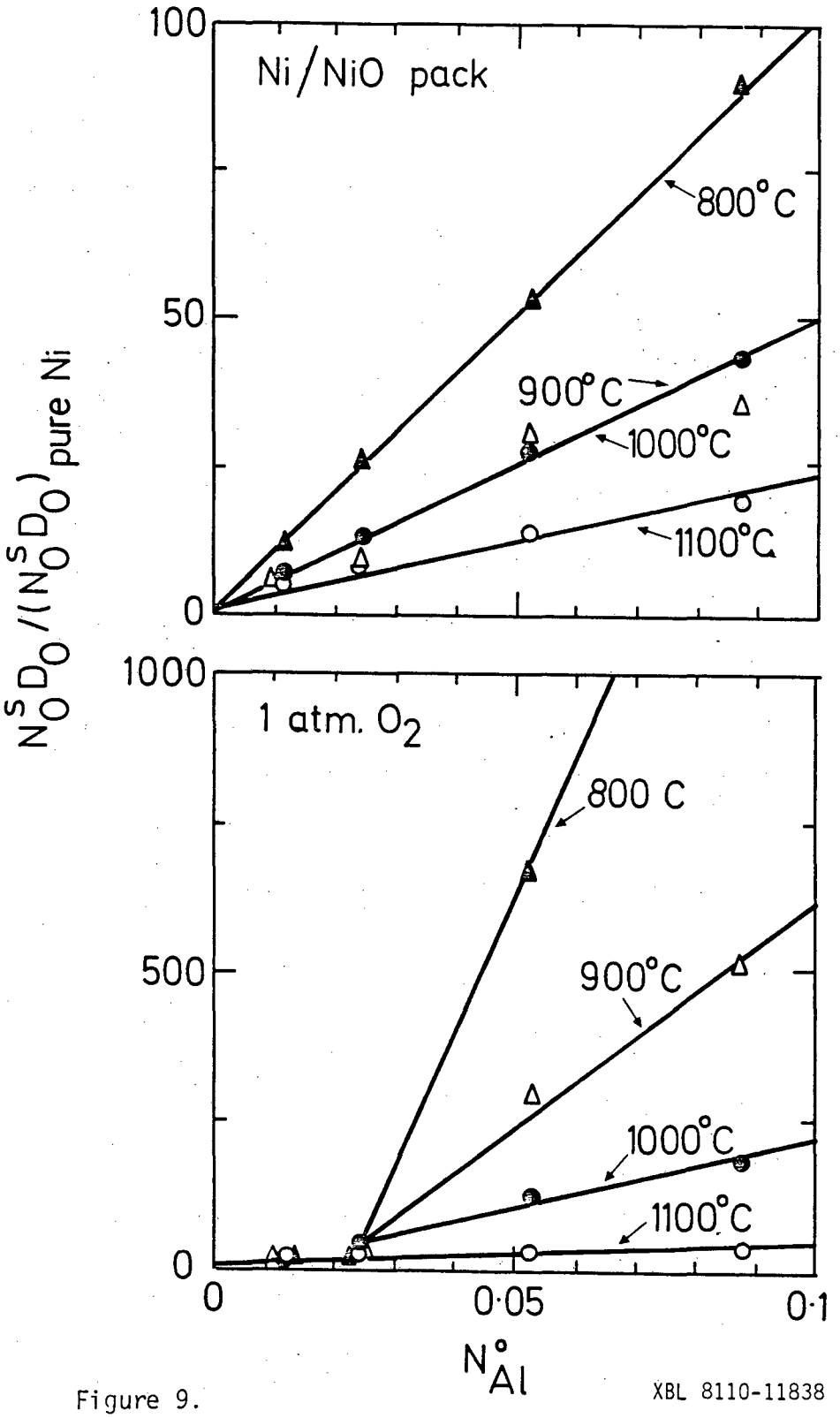

Figure 9.

XBL 8110-11838

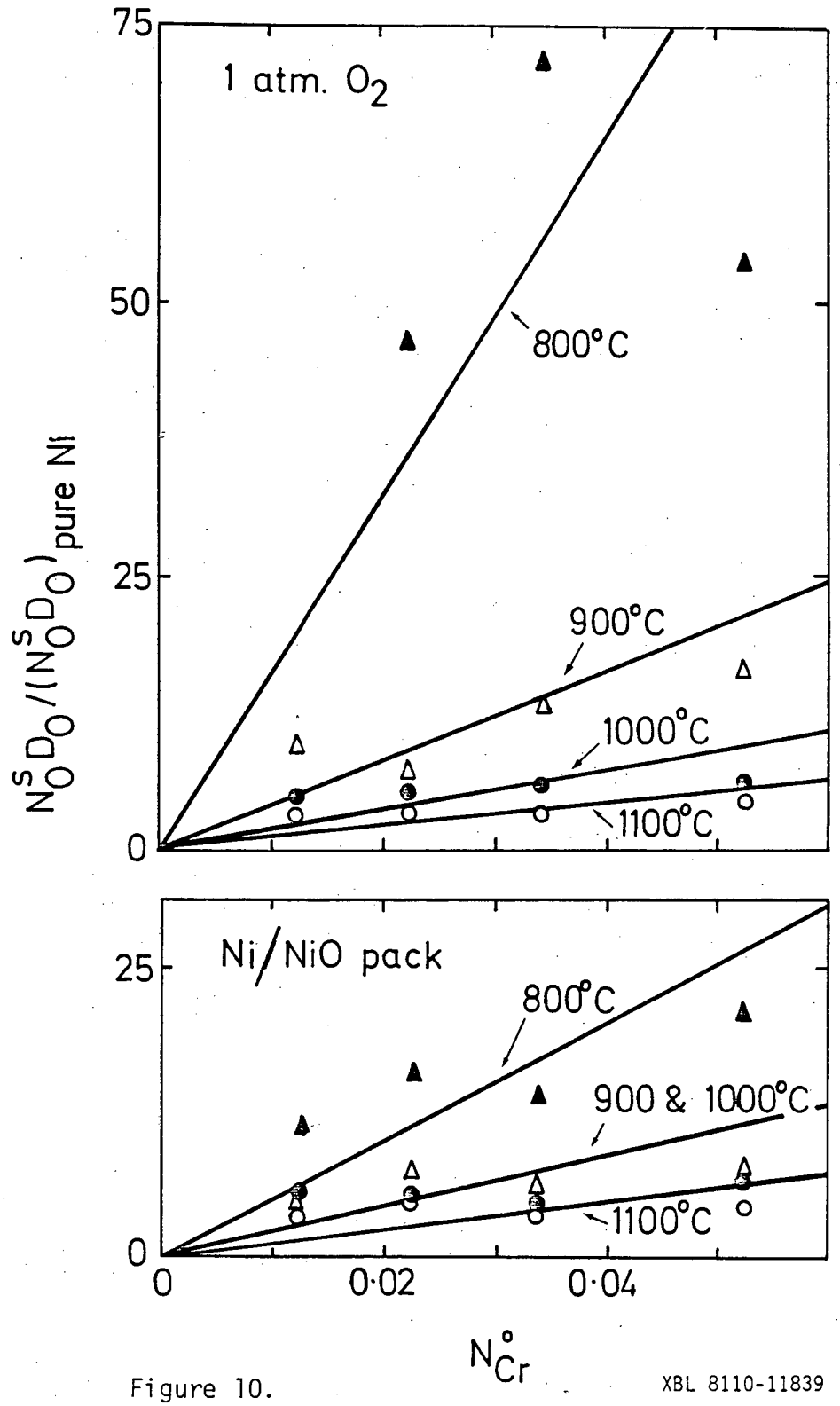

Figure 10.

XBL 8110-11839

This report was done with support from the Department of Energy. Any conclusions or opinions expressed in this report represent solely those of the author(s) and not necessarily those of The Regents of the University of California, the Lawrence Berkeley Laboratory or the Department of Energy.

Reference to a company or product name does not imply approval or recommendation of the product by the University of California or the U.S. Department of Energy to the exclusion of others that may be suitable.

TECHNICAL INFORMATION DEPARTMENT
LAWRENCE BERKELEY LABORATORY
UNIVERSITY OF CALIFORNIA
BERKELEY, CALIFORNIA 94720